https://doi.org/10.5194/egusphere-2023-2096
Preprint. Discussion started: 4 October 2023

On the sensitivity of aerosol-cloud interactions to changes in sea surface temperature in radiative-convective equilibrium

Suf Lorian[1,2] and Guy Dagan[1]

[1]Fredy and Nadine Herrmann Institute of Earth Sciences, The Hebrew University of Jerusalem, Jerusalem, Israel
[2]The Racah Institute of Physics, The Hebrew University of Jerusalem, Jerusalem, Israel

Correspondence: Guy Dagan (guy.dagan@mail.huji.ac.il)

Abstract. Clouds play a crucial role in regulating Earth's energy balance and are influenced by anthropogenic aerosol concentration (N_a) and sea surface temperature (SST) changes. However, these two factors — aerosols and SST — are typically studied independently. In this study, we employ idealized cloud-resolving, radiative-convective-equilibrium simulations to explore aerosol-cloud interactions (ACI) under different SSTs. Our findings reveal that ACIs are dependent on the prescribed SST, even at equilibrium conditions. Specifically, we show that increasing N_a leads to a decline in top-of-atmosphere (TOA) energy gain across SSTs due to changes in the cloud radiative effect, both in the short-wave and the long-wave parts of the spectrum. TOA short-wave flux changes with an increase in N_a are found to be more sensitive to the underlined SST conditions compared to long-wave radiation. The variations in how the clouds' short-wave radiative effect responds to N_a at various SSTs are explained by variations in the sensitivity of the water content in the cloud. Specifically, the sensitivity of the water content to N_a decreases with SST due to deepening of the warm, liquid portion of the cloud. This deepening results in clouds that are less responsive to aerosol-induced warm rain suppression. Furthermore, with an increase in N_a, we observe an increase in latent heat release at the upper troposphere associated with heightened production of snow and graupel. We show that this trend, which is consistent across all SSTs, affects the anvil cloud cover by affecting the static–stability at the upper troposphere via a similar mechanism to the iris–stability effect, resulting in a decline in TOA long-wave energy gain. In conclusion, under the ongoing climate change, studying the sensitivity of clouds to aerosols and SST should be conducted concomitantly as mutual effects are expected.

1 Introduction

The response of clouds to anthropogenic perturbations is highly uncertain, posing a significant challenge in predicting future climate. This uncertainty stems mainly from two aspects: 1) uncertainty regarding the change in top-of-atmosphere (TOA) radiative flux resulting from the cloud response to warming, referred to as cloud feedback (Ceppi et al., 2017), and 2) uncertainty regarding the response of clouds to anthropogenic aerosols (Bellouin et al., 2020). In the latter case, aerosols, which can serve as cloud condensation nuclei (CCN) and ice nuclei, could affect the microphysical properties and processes in clouds (Bellouin et al., 2020). Specifically, clouds forming under higher aerosol concentrations (polluted clouds) usually have initially smaller and more numerous droplets, with a narrower size distribution compared to clean clouds (Squires, 1958; Squires and

https://doi.org/10.5194/egusphere-2023-2096
Preprint. Discussion started: 4 October 2023

Twomey, 1960). The initial droplet size distribution affects the cloud's albedo (Twomey, 1974, 1977; Bellouin et al., 2020) and can affect key cloud processes such as condensation–evaporation, collision–coalescence and sedimentation (Albrecht, 1989; Seinfeld et al., 2016; Dagan et al., 2017; Heikenfeld et al., 2019; Christensen et al., 2022). These effects are known to be dependent on the environmental conditions (Gryspeerdt and Stier, 2012; Christensen et al., 2016; Dagan and Stier, 2020b), hence are expected to be state/time-dependent under ongoing climate change (Dagan et al., 2017; Igel and van den Heever, 2021; Dagan, 2022).

Ultimately, the microphysical effects mentioned above could modify the precipitation production (Albrecht, 1989). Specifically, the initiation of warm rain has been shown to be delayed and to start at higher elevations under more polluted conditions (Rosenfeld, 2000; Freud and Rosenfeld, 2012; Dagan et al., 2015; Heikenfeld et al., 2019). However, in deep convective clouds, the precipitation production could be compensated — or even over-compensated — for at higher levels of the clouds to which more water is advected under more polluted conditions (Rosenfeld et al., 2008; Koren et al., 2014; Altaratz et al., 2014). As the freezing level elevation increases with sea surface temperature (SST), at lower SSTs the warm layer (containing liquid only) of a deep convective cloud is narrower in comparison to higher SSTs. Thus, an aerosol perturbation is hypothesized to more likely suppress warm rain completely at lower SSTs than at higher SSTs, where the relatively deep warm layer of the clouds enables longer diffusional growth of the droplets to the critical size which initiates precipitation (Freud and Rosenfeld, 2012; Heikenfeld et al., 2019). Warm rain suppression and, as a consequence, enhanced freezing of this water in the cold (containing ice) sections of the cloud, will result in more latent heat release at the upper parts of the troposphere (Rosenfeld et al., 2008; Igel and van den Heever, 2021) and thus in changes in the atmospheric stability.

In addition to the effect on precipitation, it has been previously suggested that the aerosol's effect on deep convective clouds can increase the anvil cloud mass and extent by increasing the upward advection of water (Fan et al., 2010, 2013; Grabowski and Morrison, 2016; Chen et al., 2017). This trend could be explained by the convective invigoration hypothesis (Williams et al., 2002; Koren et al., 2005; Seifert and Beheng, 2006; Rosenfeld et al., 2008; Yuan et al., 2011; Koren et al., 2014). Under this hypothesis, which remains highly questionable, increasing aerosol concentrations have been suggested to drive stronger latent heat release and hence stronger vertical velocities. In addition, under high aerosol concentration conditions, the smaller hydrometeors are transported higher into the atmosphere for a given vertical velocity (Koren et al., 2015; Dagan et al., 2018, 2020), and their lifetime at the upper troposphere is longer, due to a weaker sedimentation rate (Fan et al., 2013; Grabowski and Morrison, 2016). However, it is important to note that these proposed aerosol effects are still highly uncertain (Stevens and Feingold, 2009; Varble, 2018; Romps et al., 2023).

Cloud feedback, or the response of the cloud radiative effect (CRE) to surface warming, was recently shown to depend on the assumed aerosol concentration (Dagan, 2022). In the tropics, the radiative effect of both shallow (Gettelman and Sherwood, 2016) and deep (Ceppi et al., 2017) clouds is expected to further warm the surface. Shallow tropical and sub-tropical clouds — which have a general radiative cooling effect — are expected to become less prevalent and less radiatively opaque, thus producing a general (but still highly uncertain) positive feedback (Gettelman and Sherwood, 2016; Nuijens and Siebesma, 2019). At the same time, deep tropical clouds are also expected to react to surface warming in a way that modifies their CRE (Ceppi et al., 2017). Specifically, it has been suggested that the tropical anvil cloud temperature and coverage react to surface

https://doi.org/10.5194/egusphere-2023-2096
Preprint. Discussion started: 4 October 2023

warming (Hartmann and Larson, 2002; Zelinka and Hartmann, 2010; Bony et al., 2016; Ceppi et al., 2017). Tropical anvil clouds strongly modulate the long-wave emissions of Earth as these clouds are much colder than the surface (by about 70-90K) and are generally opaque in the long-wave, thus emitting a significantly lower amount of energy to space than otherwise would be emitted without them. In addition, anvil clouds could also strongly modulate the short-wave radiation budget, depending on their optical thickness (Hartmann and Berry, 2017; Li et al., 2019; Sokol and Hartmann, 2023). Hence, any anthropogenic-driven changes to the anvil cloud properties, such as amount and temperature, could significantly affect Earth's energy budget (Zelinka and Hartmann, 2010; Ceppi et al., 2017).

A central feature of the anvil cloud response to SST changes is the fixed anvil temperature (FAT) hypothesis (Hartmann and Larson, 2002), which states that the temperature of anvil clouds is anticipated to remain roughly fixed with warming. According to the FAT hypothesis, anvil top heights are determined by clear-sky radiative cooling, which in turn is primarily determined by water vapor concentration. The water vapor concentration, following the Clausius-Clapeyron relation, sharply drops to negligible values near the temperatures of the upper-troposphere, making the radiative cooling inefficient above this level and still efficient below this level. In a clear-sky free troposphere, radiative cooling is balanced by adiabatic warming due to subsiding motions, thus the energy budget can be formulated as follows:

$$Q_r = -S\omega \tag{1}$$

where Q_r is the radiative cooling rate, ω is the vertical pressure velocity, and S is the static-stability defined as:

$$S = -\frac{T}{\theta}\frac{\partial \theta}{\partial P} \tag{2}$$

where T is the air temperature, θ is the potential temperature and P is the pressure.

The subsidence motion below the sharp drop in radiative cooling and the lack of subsidence above this level generates vertical divergence in the clear sky, which, due to conservation of mass, is balanced by horizontal divergence from the convective regions. This convective divergence controls anvil clouds (Hartmann and Larson, 2002; Zelinka and Hartmann, 2011, 2010; Bony et al., 2016) (Below, in Fig. 5, vertical profiles of S, Q_r, ω and its vertical divergence are presented).

Beside increasing in height (while maintaining nearly fixed temperatures), anvil clouds are predicted by global climate models, high-resolution convective-permitting models and observations to decrease with surface temperature (Lindzen et al., 2001; Zelinka and Hartmann, 2011; Mauritsen and Stevens, 2015; Bony et al., 2016; Williams and Pierrehumbert, 2017; Wing et al., 2020; Saint-Lu et al., 2020; Beydoun et al., 2021). The mechanisms behind this decrease in anvil cloud coverage rely on the same physics as do the mechanisms of the FAT hypothesis. Namely, it has been suggested that as the climate warms, the clouds rise, but find themselves in a more stable atmosphere (while remaining at nearly the same temperature). This enhanced stability under warmer conditions reduces the convective outflow in the upper troposphere and hence decreases the anvil cloud fraction (Bony et al., 2016; Beydoun et al., 2021). Specifically, it was shown that the maximum of the radiative-driven mass divergence in convective regions (D_r), defined as:

$$D_r = \frac{\partial \omega}{\partial P} \tag{3}$$

https://doi.org/10.5194/egusphere-2023-2096
Preprint. Discussion started: 4 October 2023

can accurately predict the anvil cloud fraction, and decreases with the increase in stability occurring with an increase in SST (Bony et al., 2016; Beydoun et al., 2021). In addition to the radiative-driven divergence, slow evaporation (Seeley et al., 2019) and sedimentation (Beydoun et al., 2021) of the ice crystals at the upper troposphere contribute to anvil cloud formation. However, changes in the lifetime of anvil clouds — determined by changes in sedimentation and evaporation — were shown to play a secondary role in the response of anvil clouds to warming (Beydoun et al., 2021).

In this study, we focus on the synergistic SST and aerosol effects on tropical convective clouds, and specifically on the CRE, under equilibrium conditions using idealized cloud-resolving, radiative-convective-equilibrium (RCE) simulations.

2 Methods

2.1 Model description

The model used in this study is the System for Atmospheric Modeling (Khairoutdinov and Randall, 2003, SAM) version 6.11.7. The microphysics scheme used is the two-moment bulk microphysics of Morrison et al. (2005). The aerosols available for activation are represented by a power law function of the super-saturation (SS): CCN = $N_a SS^k$, where N_a is the concentration of CCN available at 1% super-saturation and k is a constant, here equal to 0.4, representing typical maritime conditions. CCN activation at the cloud base is parameterized using the vertical velocity and CCN spectrum parameters (Twomey, 1959). In this case, we use different N_a concentrations for representing changes in aerosol concentration. Direct interactions between aerosols and radiation are not considered here, however, aerosols could affect the radiation via modifying the clouds' properties. In order to represent the Twomey effect (Twomey, 1977), the model is configured to pass cloud water and ice-crystal effective radii from the microphysics scheme to the radiation scheme.

2.2 Experimental design

The simulations used here generally follow the Radiative-Convective-Equilibrium Model Intercomparison Project (Wing et al., 2018, RCEMIP) small domain protocol but with changes in aerosol concentration. The simulations are run in a small domain, of 96×96 km^2, in order to avoid the effects of convective self-aggregation (Muller and Held, 2012; Lutsko and Cronin, 2018). The simulations are conducted with a horizontal grid spacing of 1 km, 68 vertical levels between 25 m and 31 km, and a vertical grid spacing increasing from 50 m at the surface to around 1 km at the domain top. To get solar-insulation close to the tropical-mean value, the solar radiation is fixed at 551.58 W m^{-2}, with a zenith angle of 42.05°(Wing et al., 2018). In order to initialize convection, a small thermal noise is added near the surface at the beginning of each simulation.

The concentration of CO_2 is fixed at pre-industrial level (280 ppm), while there are 25 different N_a and SSTs combinations, 5 different values for each. N_a ranges from 20 to 2000 cm^{-3} (20, 100, 200, 1000, and 2000 $^{-3}$), and the SST ranges from 290 to 310 K in 5 K intervals. This wide range of aerosol and SST conditions are used to maximize the effects and for establishing a better physical understanding. The vertical profile of O_3's represents a typical tropical atmosphere (Wing et al., 2018). For simplicity, the effect of other trace gases (such as CH_4 and N_2O) is neglected. The temporal resolution of the simulations is 10

https://doi.org/10.5194/egusphere-2023-2096
Preprint. Discussion started: 4 October 2023

seconds, and of the interactive radiative scheme is 5 minutes (using the CAM radiation scheme (Collins et al., 2006)). All fields have an output resolution of 1 hour; 3-D fields are saved as snapshots, while domain statistics are saved as hourly averages. Each simulation was run for 150 days (Wing et al., 2018), and the last 30 days of each simulation were used for statistical analysis.

3 Results and discussion

3.1 Response of radiative and clouds' properties to aerosol perturbation under different SSTs

We start by examining the effect of changes in N_a on the TOA energy gain under different SSTs (ΔR; Fig. 1a). This figure illustrates that for all SSTs, an increase in N_a decreases ΔR, an effect which becomes stronger with a decrease in the SST. Both the long-wave (LW) and short-wave (SW) components of ΔR are negatively affected by N_a (each declining up to 4–5 W m^{-2} for the entire N_a range considered here, depending on the SST; Fig. 1b and c), with ΔR^{SW} being more susceptible to SST changes (Fig. 1c), and ΔR^{LW} decreases in a roughly similar manner across all SSTs (Fig. 1b). Moreover, the CRE (calculated as all sky radiative flux minus clear sky radiative flux) is identified as the main driver of ΔR variations, while changes in clear sky radiation has a minimal impact, as indicated by Fig. 1d–f.

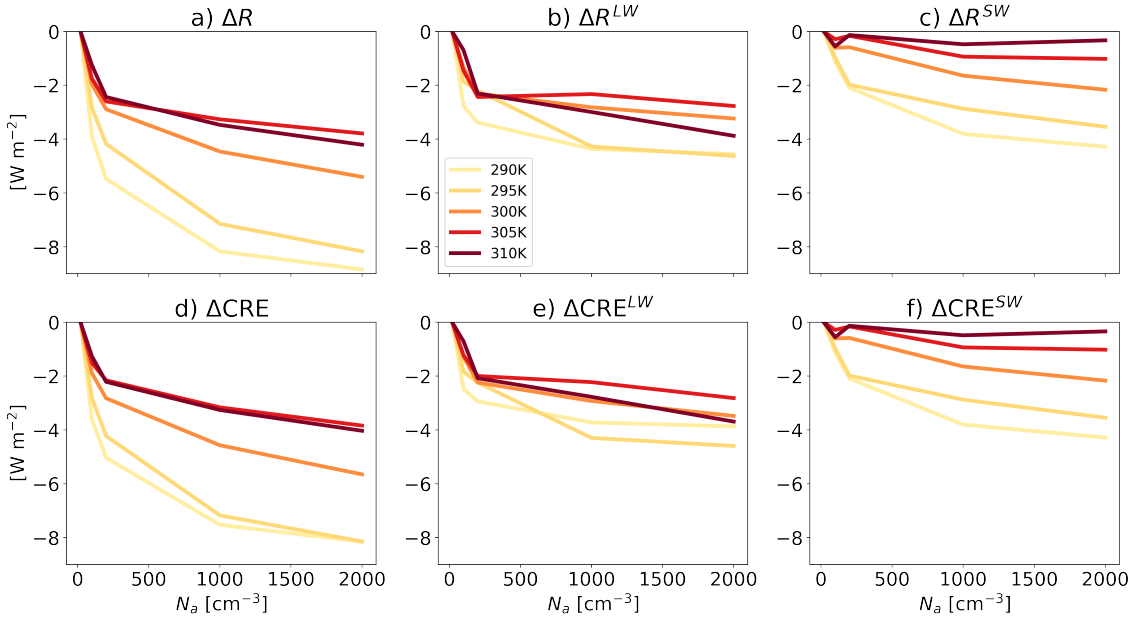

Figure 1. Changes in the domain and time mean radiative fluxes at the top of the atmosphere due to changes in aerosol concentrations (N_a). (**a**) presents the total change in radiation, while (**b**) and (**c**) present changes in long-wave (LW) and short-wave (SW) radiation, respectively. (**d**-**f**) present the changes in the total cloud radiative effect (CRE) and its LW and SW components, respectively. The values are presented relative to the cleanest run (N_a = 20 cm^{-3}) for each SST, as indicated by the Δ sign.

https://doi.org/10.5194/egusphere-2023-2096
Preprint. Discussion started: 4 October 2023

Figure 2 presents vertical profiles (as a function of temperature) of cloud fraction and total water in the cloud for the cleanest runs (N_a = 20 cm^{-3}; panels a and b), and their response to increasing N_a to 2000 cm^{-3}, relative to the cleanest run for each SST (as indicated by the Δ sign; panels c and d). With an increase in N_a, the amount of total water (containing all hydrometeors) in the cloud increases mostly in the warm section of the cloud (at temperatures above roughly 260 K; Fig. 2d). The increase in total water with N_a is more pronounced for lower SSTs, with a relative increase ranging from 20% to 35% for the different N_a values used here (see Fig. S1, SI) when compared to the cleanest runs. These comparisons are made under an SST of 290K and are evaluated at the height of the maximum change. By contrast, in the highest SST case (310K), the relative increase for the different N_a ranges from 8% to 27%.

With an increase in SST, the isotherm height increases, hence, the warm section of the clouds becomes thicker. Thus, under higher SSTs, cloud droplets are more likely to grow by diffusion to the critical size that will initiate precipitation (Freud and Rosenfeld, 2012) before crossing to the cold portion of the cloud where it freezes. Since an increase in N_a acts to push warm rain formation to higher levels (Rosenfeld, 2000; Freud and Rosenfeld, 2012; Heikenfeld et al., 2019), under lower SSTs, for which the warm section of the cloud is relatively shallow (about 1250 m in the coldest case considered here), an increase in N_a can completely suppress warm rain (see Fig. 3g). In contrast, under higher SSTs, for which the warm section of the cloud is relatively deep (about 6000 m in the warmest case considered here), an increase in N_a drives warm rain suppression at the lower levels, which is compensated for at higher levels of the warm section (Fig. 3g). Because the delay in warm rain is not offset at higher levels within the warm section of the cloud under low SSTs, the rise in water content within the warm section of the cloud with an increase in N_a is more pronounced under low SST conditions compared to high SST conditions (Fig. 2d). The stronger increase in total water with N_a under lower SSTs leads to the stronger SW reflectivity, i.e., a decrease in ΔR^{SW}, as can be seen in Fig. 1c. Furthermore, the stronger increase in total water with N_a under lower SSTs is manifested in an increase in the domain and time mean liquid water path (LWP; Fig.4a). In addition, the warm rain suppression under higher N_a and lower SSTs results in more super-cooled water (Fig. 3f) (Carrió et al., 2011; Chen et al., 2017), leading to higher production of snow (Fig. 3j) (Chen et al., 2017), and drives higher riming rates, thus producing more graupel (Fig. 3i) (Chen et al., 2017).

Another observation from Fig. 2c is that an increase in N_a drives a decrease in anvil cloud fraction, consistently across all SSTs. The reduction in anvil cloud fraction with N_a is accompanied by a reduction in the domain and time mean ice water path (IWP; Fig. 4b). The decrease in IWP with an increase in N_a is also consistent with the reduction in cloud ice at the upper troposphere (Fig. 3f), which appears consistently across all SSTs.

In order to understand the reduction in anvil cloud fraction with N_a, as can be seen in Fig. 2c, next we examine the sensitivity of the maximum (in the vertical dimension – see Fig. 5d) of the radiative-driven mass divergence (Bony et al., 2016, D_r) to N_a under the different SSTs (Fig. 6). Figure 6a illustrates that the anvil cloud fraction (defined as the domain and time mean cloud fractions at temperatures below 245K) is strongly correlated with D_r (Pearson correlation coefficient $\approx$ 0.96 with a P-value $<$ 0.01). While the general decrease in D_r with SST has previously been demonstrated (Bony et al., 2016), here we show that for a given SST, D_r generally decreases with N_a (Fig. 6b). The general reduction in D_r with N_a drives a general reduction

https://doi.org/10.5194/egusphere-2023-2096
Preprint. Discussion started: 4 October 2023

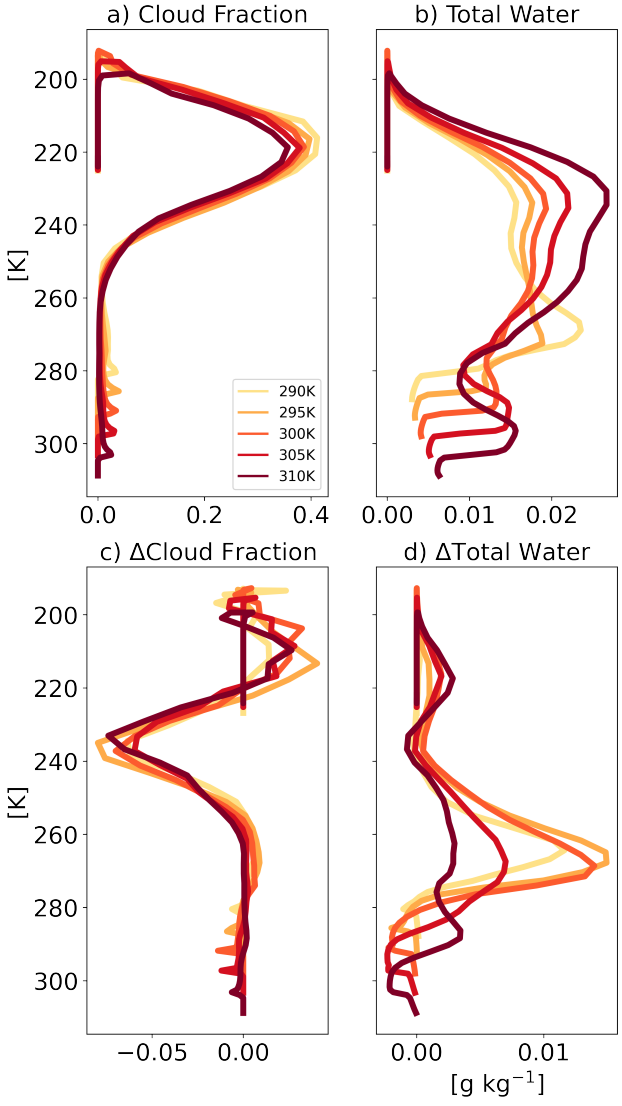

Figure 2. Domain and time mean vertical profiles of cloud fraction and total water in the cloud for the baseline, cleanest runs (N_a = 20 cm^{-3}; **a** and **b**, respectively), and their response to increasing N_a to 2000 cm^{-3}, relative to the cleanest run for each SST (**c** and **d**, respectively). Here we only present the baseline and the response of the most polluted runs for clarity. The full range of N_a is presented in Fig. S1, SI.

in anvil cloud fraction with N_a for a given SST (Fig. 6c). This reduction in D_r and anvil cloud fraction with N_a explains the reduction in IWP with N_a (Fig. 4b), which in turn can explain the reduction in ΔR^{LW} (Fig. 1b).

A reduction in D_r with N_a could be attributed to changes in Q_r (the radiative cooling rate; Fig. 5b) and/or in the static-
170 stability (S; Fig. 5a). Thus, in order to understand the reasons behind the decrease in D_r with N_a (for a given SST), in Fig. 7 we calculate the change in D_r with N_a for the different SSTs, assuming that either Q_r or S is held fixed at the value it attains

https://doi.org/10.5194/egusphere-2023-2096
Preprint. Discussion started: 4 October 2023

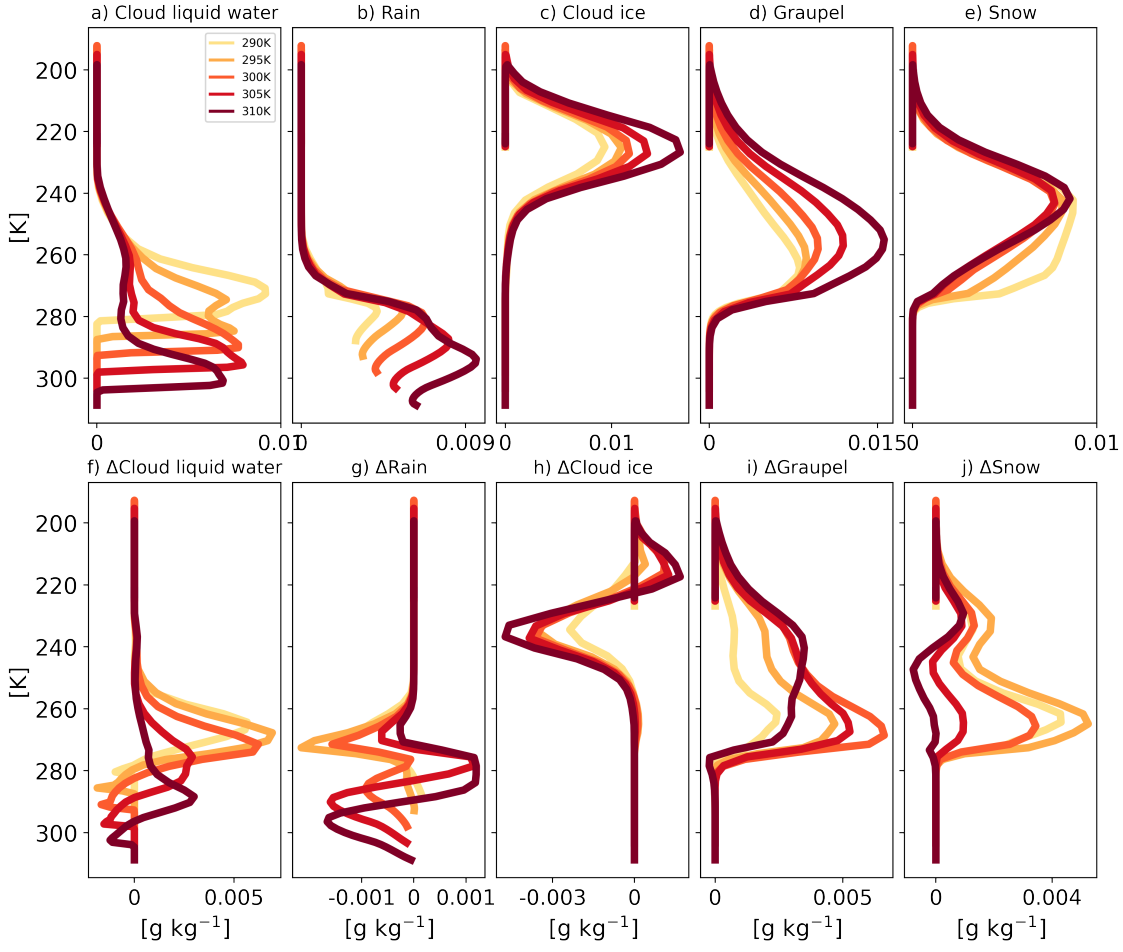

Figure 3. Domain and time mean vertical profiles of the different hydrometeors for the baseline, cleanest runs (N_a = 20 cm^{-3}): (**a**) cloud liquid water, (**b**) rain, (**c**) ice, (**d**) graupel, and (**e**) snow, and their response to increasing N_a to 2000 cm^{-3}, relative to the cleanest run for each SST (**f** – **j**). Here we only present the baseline and the response of the most polluted runs for clarity. The full range of N_a is presented in Fig. S2, SI.

at a reference N_a of 200 cm^{-3} for each SST. This calculation is similar to that presented in Fig. 4 of Bony et al. (2016), but for changes in N_a instead of in SST. Figure 7 illustrates that the reduction of D_r with an increase in N_a can mostly be attributed to changes in S. This result is illustrated by the consistent reduction in D_r with N_a for all SSTs when only S (or the temperature – T) is varied. However, when only Q_r is varied, the trend of D_r with N_a is not consistent across the different SSTs, and for some of the SSTs, the trend is not monotonic.

The domain and time mean temperature vertical profiles for the different simulations and their response to an increase in N_a is presented in Fig. 8. This figure illustrates that for a given SST, an increase in N_a drives strong warming of the upper

https://doi.org/10.5194/egusphere-2023-2096
Preprint. Discussion started: 4 October 2023

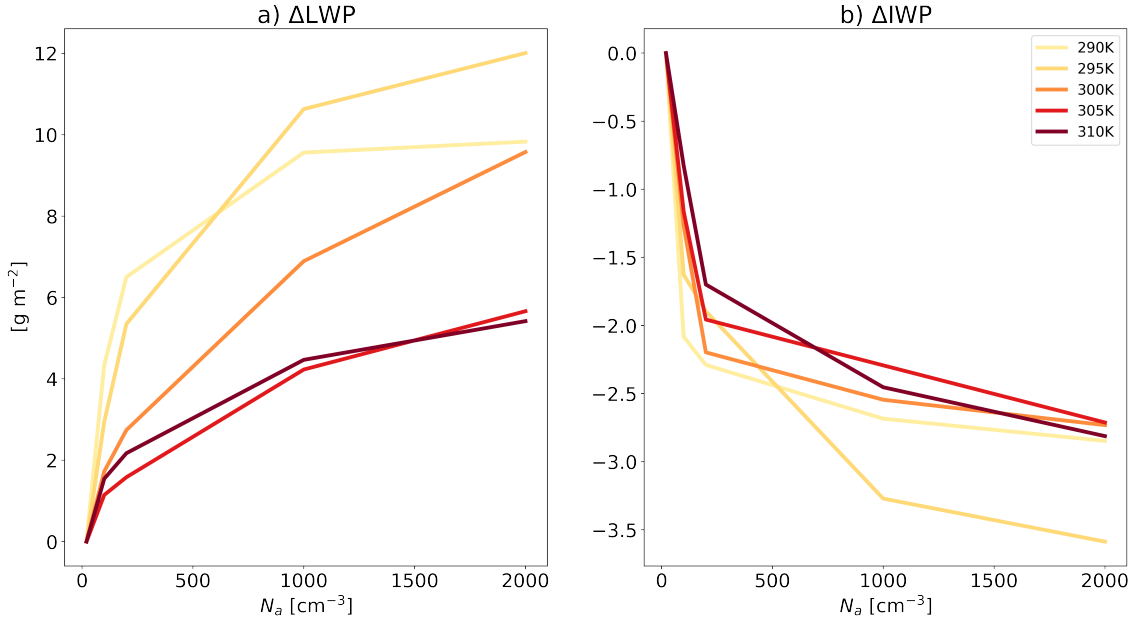

Figure 4. The response of domain and time mean liquid water path (LWP; **a**) and ice water path (IWP; **a**) to an increase in N_a, relative to the cleanest run for each SST (N_a = 20 cm^{-3}).

troposphere and a weak cooling of the lower troposphere. This trend is consistent with the increase in S with N_a (Fig. 5a), which in turn explains the reduction in the anvil cloud fraction.

A remaining open question concerns the reasons behind the strong warming of the upper troposphere (or behind the increase in S) with N_a. In the model, a central prognostic variable is the liquid/ice water static energy (h_L). The h_L tendency equation contains 5 terms: advection (adv), radiation (rad), latent heating (latent), turbulence and large-scale tendency (Khairoutdinov and Randall, 2003). In an RCE configuration, by definition, the large-scale tendency is set to zero, thus having no effect here. In addition, in our simulations the turbulence term is negligible compared to the rest of the terms. Hence, in Fig. 9 we present vertical profiles of the domain and time mean $\frac{\partial h_L}{\partial t}$ due to latent heating, advection, and radiation in the different simulations. This figure illustrates that under equilibrium conditions, the latent heating acts to heat the upper troposphere, advection acts to cool it, although by a smaller magnitude, and radiation acts to weakly cool the entire troposphere almost uniformly. This trend is enhanced with an increase in N_a (Fig. 9d-f), suggesting that the increase in temperature of the upper troposphere with N_a is driven by a stronger latent heat release, which is in turn driven by higher production rates of graupel and snow with N_a (Figs. 3i and j). Graupel and snow, unlike small ice crystals, efficiently sediment out of the cold portion of the cloud, thus leaving behind the heat they released in their formation, resulting in a net warming effect. Therefore, higher production of graupel and snow with N_a is identified as the main driver of the observed temperature increase in the upper troposphere.

https://doi.org/10.5194/egusphere-2023-2096
Preprint. Discussion started: 4 October 2023

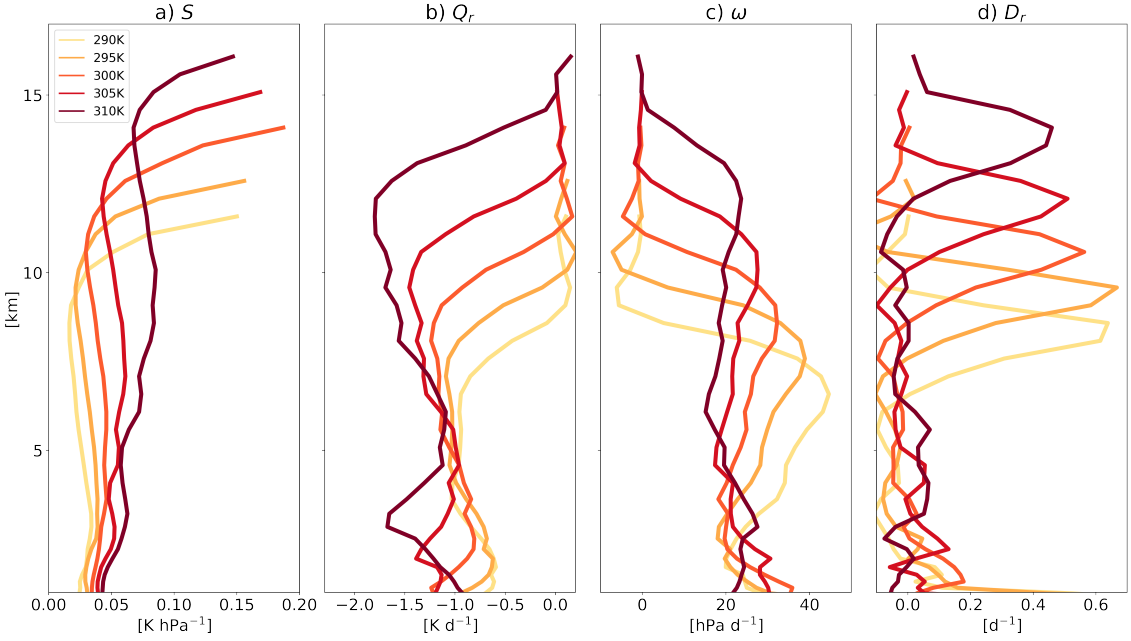

Figure 5. Domain and time mean vertical profiles of the: **a)** static-stability – S, **b)** radiative cooling rate – Q_r, **c)** vertical pressure velocity – ω, and **d)** radiative-driven mass divergence – D_r for the different simulations conducted under N_a = 20 cm^{-3} and different SST conditions. Here we only present the baseline for clarity. The full range of N_a is presented in Fig. S3, SI.

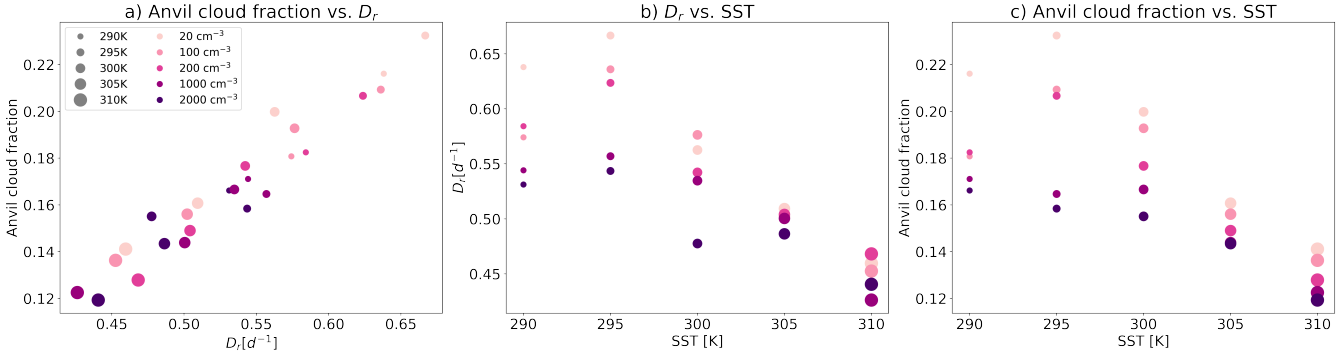

Figure 6. Changes in domain and time mean anvil cloud fraction with D_r for the different simulations conducted under different N_a and SST (**a**), changes in D_r with SST (**b**), and changes in anvil cloud fraction with SST (**c**).

3.2 Examining the surface precipitation response to aerosol perturbation using the atmospheric energy budget

195 Next, we examine the response of the surface precipitation to N_a under the different SSTs. Figure 10a illustrates an increase in surface precipitation (in energy units – $L\Delta SP$, where L is the latent heat of vaporization and SP is the surface precipitation) with N_a across SSTs. In order to understand this increase, we use the atmospheric energy budget perspective (Muller and

https://doi.org/10.5194/egusphere-2023-2096
Preprint. Discussion started: 4 October 2023

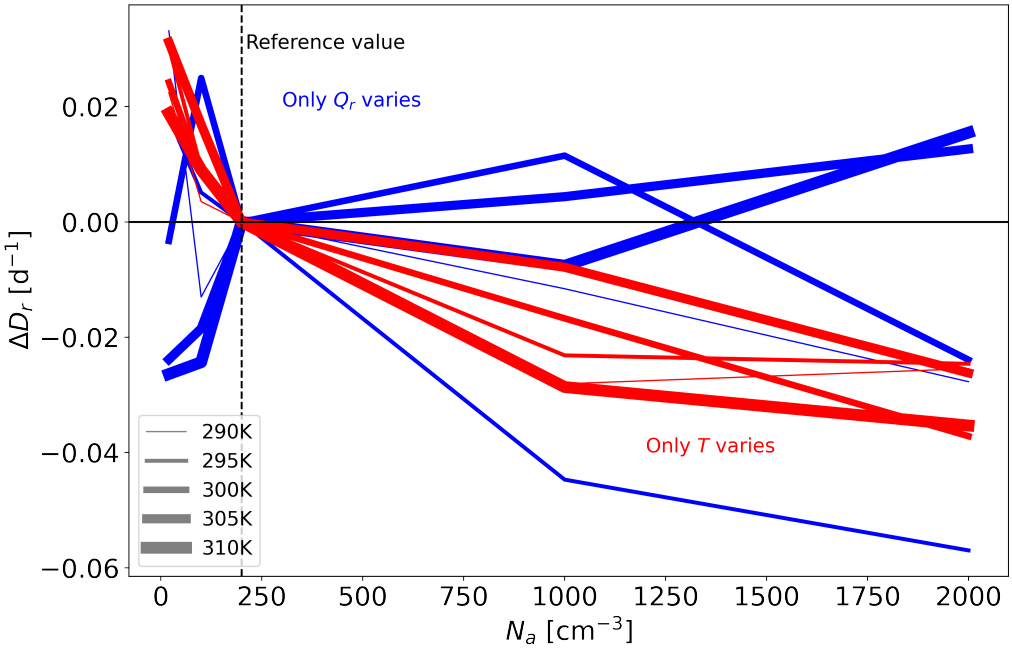

Figure 7. Relationship between the radiative-driven divergence (D_r) and N_a diagnosed by assuming that only either the temperature profile (T – red curves) or the clear-sky radiative cooling profile (Q_r – blue curves) vary with N_a. The reference for the T and Q_r are the simulations conducted under N_a = 200 cm^{-3} (dashed vertical line) for each SST.

O'Gorman, 2011; Dagan and Stier, 2020a; Williams et al., 2023) and decompose the changes in $L\Delta SP$ to changes in long-wave atmospheric radiative cooling (ΔLWC, calculated as the TOA's LW radiation flux minus the surface's net LW radiation flux; Fig. 10b), changes in surface sensible heat flux (ΔSHF; Fig. 10c), and changes in atmospheric short-wave absorption (ΔSWA, calculated as the TOA's net SW radiation flux minus the surface's net SW radiation flux; Fig. 10d), following the notations of Williams et al. (2023):

$$L\Delta SP = \Delta LWC - \Delta SWA + \Delta SHF \tag{4}$$

We note that Eq. 4 holds under equilibrium conditions, as simulated here (Muller and O'Gorman, 2011; Dagan and Stier, 2020a). Following the notations of Eq. 4, Fig. 10a can be reconstructed by summing Fig. 10b-d. Hence, we note that the increase in $L\Delta SP$ could mostly be explained by enhanced ΔLWC (driven by enhanced outgoing LW radiation; Fig. 10b), while changes in ΔSWA produce only a small positive contribution, and changes in ΔSHF present a small and non-consistent across SSTs contribution. The enhanced ΔLWC with N_a is driven by the decreased anvil cloud fraction with N_a across SSTs, as illustrated in Fig. 2c, and is consistent with the reduction in ΔR^{LW} presented in Fig. 1. These results suggest that under

https://doi.org/10.5194/egusphere-2023-2096
Preprint. Discussion started: 4 October 2023

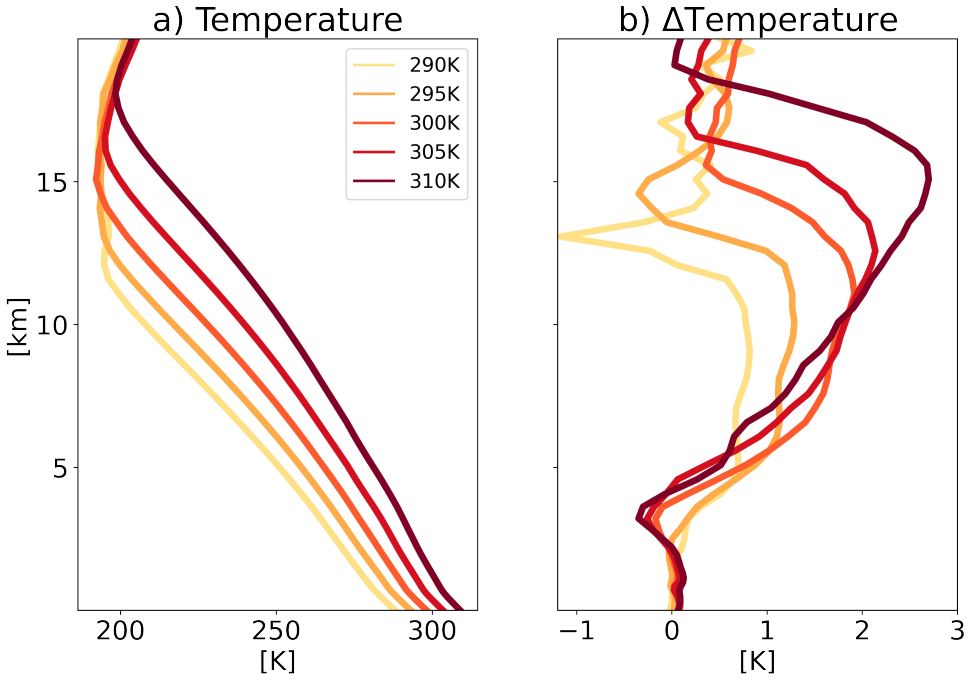

Figure 8. Domain and time mean vertical profiles of temperature for the baseline, cleanest runs (N_a = 20 cm^{-3}; **a**) and its response to increasing N_a to 2000 cm^{-3}, relative to the cleanest run for each SST (**b**). Here we only present the baseline and the response of the most polluted runs for clarity. The full range of N_a is presented in Fig. S5, SI.

equilibrium conditions, higher N_a concentrations drive higher long-wave cooling rates of the atmospheric column, which supports the production of more precipitation.

4 Conclusions

Under anthropogenic-driven climate change, Earth's energy budget is influenced by changes in the atmospheric composition, including anthropogenic aerosols, which could affect the cloud radiative properties. In addition, changes in SST could drive changes in the cloud radiative properties as well, which can in turn further change the SST. In this study, we investigate the combined impact of SST and aerosol concentration (N_a) on cloud properties in the framework of high-resolution radiative-convective-equilibrium (RCE) simulations.

Using these idealized RCE simulations, we demonstrate that increasing N_a decreases top-of-atmosphere (TOA) energy gain across all SSTs, both in the long-wave (LW) and short-wave (SW) parts of the spectrum, as a result of changes in the cloud radiative effect. We also show that this effect is stronger under lower SSTs, contributed mostly by a stronger SW response. As

https://doi.org/10.5194/egusphere-2023-2096
Preprint. Discussion started: 4 October 2023

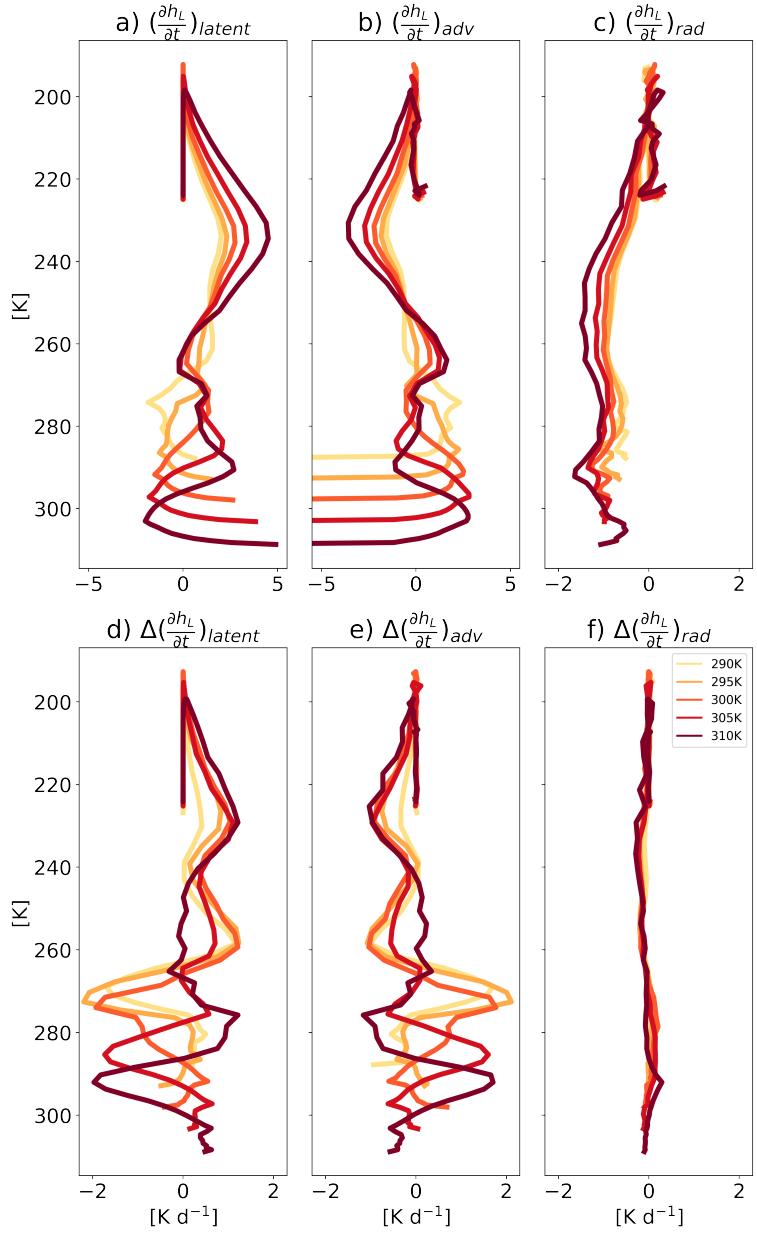

Figure 9. Vertical profiles of the domain and time mean tendency of the liquid/ice water static energy for the baseline, cleanest runs (N_a = 20 cm^{-3}) (h_L) due to (**a**) latent heating, (**b**) advection, and radiation (**c**) in the different simulations conducted under different SST and N_a. Panels **d** – **f** presents the response of these terms to increasing N_a to 2000 cm^{-3}, relative to the cleanest run for each SST. Here we only present the baseline and the response of the most polluted runs for clarity. The full range of N_a is presented in Fig. S5, SI.

https://doi.org/10.5194/egusphere-2023-2096
Preprint. Discussion started: 4 October 2023

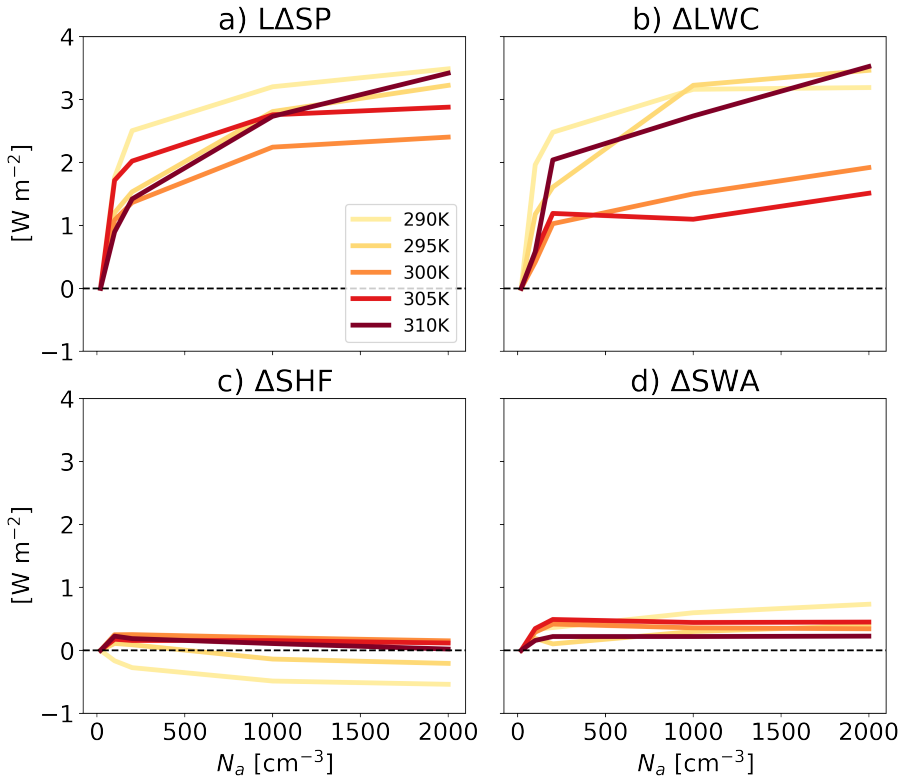

Figure 10. The response of domain and time mean surface precipitation ($L\Delta SP$; **a**), long-wave atmospheric radiative cooling (ΔLWC; **b**), surface sensible heat flux (ΔSHF; **c**) and atmospheric short-wave absorption (ΔSWA; **d**) to an increase in N_a, relative to the cleanest run for each SST (N_a = 20 cm^{-3}).

known from previous studies, increasing N_a pushes warm rain initiation to higher levels of the cloud (Freud and Rosenfeld, 2012; Heikenfeld et al., 2019). Under low SSTs, where the warm section of the cloud is relatively shallow (as depicted by the arrows numbered as 1 in the schematic figure, Fig. 11), this vertical delay in warm rain formation means that liquid cloud droplets cross the freezing level before having time to sufficiently grow and initiate precipitation (as depicted by arrow 2 in Fig. 11). As a result, this process directly leads to an increase in the water content in the warm section of the cloud. In contrast, under high SSTs, where the warm section of the cloud is relatively deep, the delay in warm rain formation can be compensated for at higher (but still warm) levels of the cloud due to sufficient time and space for liquid cloud droplets to initiate precipitation (as depicted by arrow 3 in Fig. 11). Hence, the liquid water content in clouds developing under warmer SSTs is less sensitive to N_a. The increase in water content with an increase in N_a under low SST, results in more SW reflection back to space compared with higher SSTs. This trend explains the SST-sensitivity of the SW response to N_a.

On the other hand, the decrease in the TOA energy gain in the LW part of the spectrum with an increase in N_a (ΔR^{LW}) is a consequence of a reduction in anvil cloud fraction. As has been previously reported, (Bony et al., 2016), we observe a strong

https://doi.org/10.5194/egusphere-2023-2096
Preprint. Discussion started: 4 October 2023

correlation between the anvil cloud fraction and the maximum radiative-driven mass divergence at the upper troposphere (D_r). We demonstrate that D_r decreases with N_a for a given SST, which drives the reduction in anvil cloud fraction. The reduction in D_r with an increase in N_a is shown here to be driven by an increase in static-stability at the upper troposphere under more
235 polluted conditions. The decrease in anvil cloud fraction with N_a across SSTs (as depicted by arrow 4 in Fig. 11) leads to a decline in ice water path (IWP), causing an increase in the outgoing LW radiation, i.e., decreasing ΔR^{LW}. This reduction in ΔR^{LW} at the TOA directly increases LW cooling of the atmospheric column (ΔLWC), which, in turn, is identified as the main driver of enhanced surface precipitation ($L\Delta SP$).

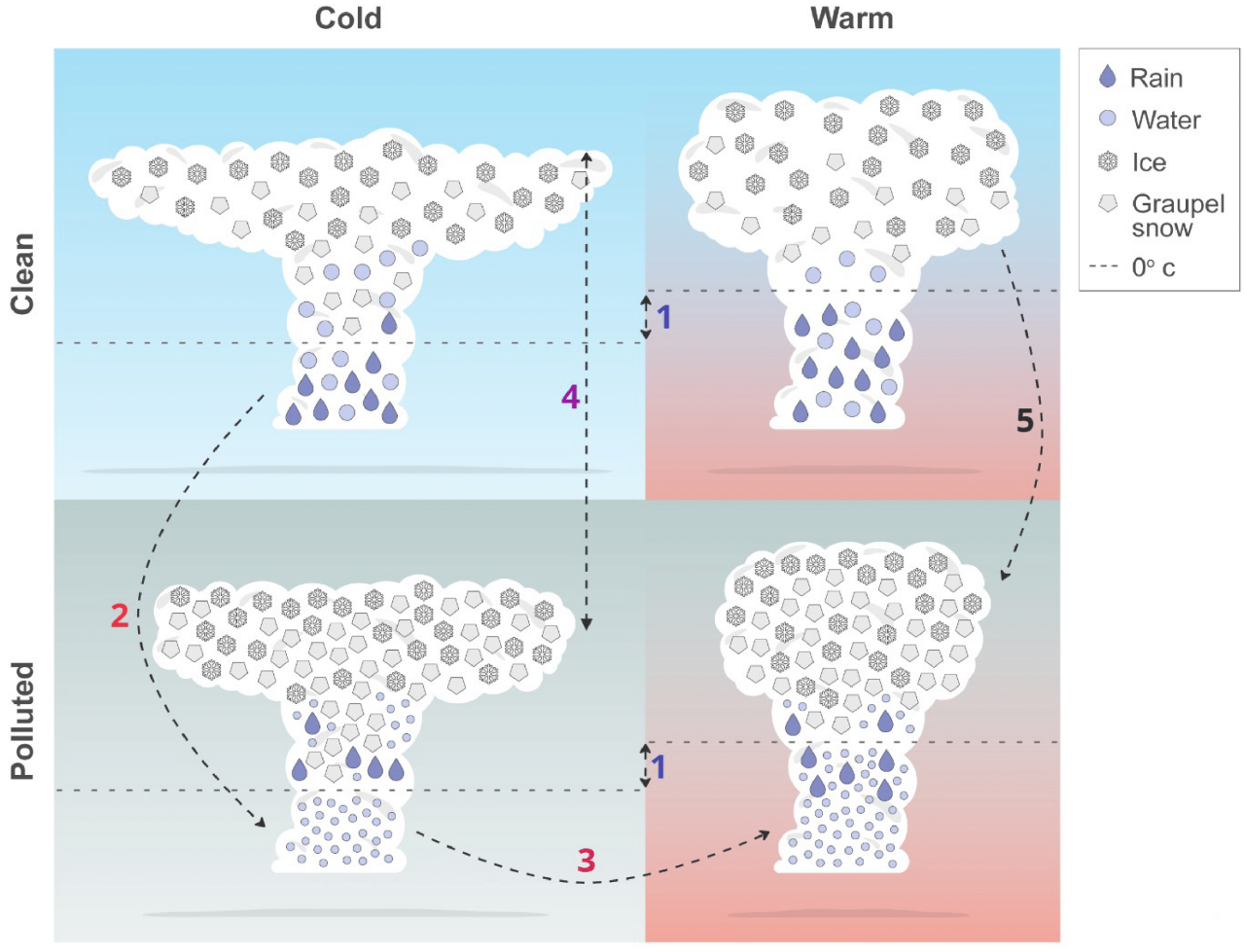

Figure 11. Schematic representation of a cold SST, hot SST, clean and polluted runs, and their respective cloud fraction, hydrometeors' size and distribution in the cloud, and thickness of the warm part of the cloud.

https://doi.org/10.5194/egusphere-2023-2096
Preprint. Discussion started: 4 October 2023

Lastly, we try to explain the observed relative warming of the upper troposphere with N_a, which is consistent with the rise in static-stability, by examining the tendency equation of liquid/ice water static energy ($\frac{dh_L}{dt}$). We demonstrate that the increase in static-stability with N_a can be explained by an increase in the latent-heating of the upper troposphere. The warm rain suppression with N_a leads to heightened production rates of graupel and snow (as depicted by arrow 5 in Fig. 11), which efficiently sediment out from the colder region of the cloud. As they descend, they leave behind the latent heat released during their formation, resulting in an overall warming effect and an increased stability.

The results presented here are based on idealized RCE simulations in a small domain, which suppress convective self-aggregation and large-scale circulation. Hence, in future work we aim to examine our conclusion in a set of simulations conducted using a channel domain, which includes interactions with larger scales. Furthermore, the role of other modeling choices, such as horizontal and vertical resolution and the role of boundary conditions (Dagan et al., 2022) in our results should be examined in future work. In addition, in this work we excluded aerosol-radiation interactions, which could drastically alter TOA energy gain (Bellouin et al., 2020; Williams et al., 2023), and as such could be of interest. Finally, our work is based on single-model simulations. An RCEMIP stage focusing on aerosol effect on clouds and RCE climate is currently being conducted. This set of multi-model simulations under harmonized setup will allow us to confront our conclusions with a large variety of models and microphysical schemes.

This work suggests that under equilibrium conditions, the magnitude of the effective radiative forcing by aerosol-cloud interactions decreases (becomes less negative) with an increase in SST. These results predict that under the ongoing global warming trend, the ability of ACI to counteract some of the positive radiative forcing by greenhouse gasses will become smaller with time. In addition, it suggests that studying the sensitivity of clouds to aerosol and SST should be conducted concomitantly as mutual effects are expected.

Code and data availability. SAM is publicly available at: http://rossby.msrc.sunysb.edu/ marat/SAM.html The data presented in this study is publicly available at: https://doi.org/10.5281/zenodo.8338310

Author contributions. SL carried out the simulations and analyses presented. GD assisted with the simulations. SL and GD designed and interpreted the analyses. SL prepared the manuscript with contributions from GD.

Competing interests. At least one of the (co-)authors is a member of the editorial board of Atmospheric Chemistry and Physics

Acknowledgements. This research was supported by the Israel Science Foundation (grant number: 1419/21).

https://doi.org/10.5194/egusphere-2023-2096
Preprint. Discussion started: 4 October 2023

References

Albrecht, B. A.: Aerosols, cloud microphysics, and fractional cloudiness, Science, 245, 1227–1230, 1989.

Altaratz, O., Koren, I., Remer, L., and Hirsch, E.: Cloud invigoration by aerosols—Coupling between microphysics and dynamics, Atmospheric Research, 140, 38–60, 2014.

Bellouin, N., Quaas, J., Gryspeerdt, E., Kinne, S., Stier, P., Watson-Parris, D., Boucher, O., Carslaw, K. S., Christensen, M., Daniau, A.-L., et al.: Bounding global aerosol radiative forcing of climate change, Reviews of Geophysics, 58, e2019RG000 660, 2020.

Beydoun, H., Caldwell, P. M., Hannah, W. M., and Donahue, A. S.: Dissecting anvil cloud response to sea surface warming, Geophysical Research Letters, 48, e2021GL094 049, 2021.

Bony, S., Stevens, B., Coppin, D., Becker, T., Reed, K. A., Voigt, A., and Medeiros, B.: Thermodynamic control of anvil cloud amount, Proceedings of the National Academy of Sciences, 113, 8927–8932, 2016.

Carrió, G., , and Cotton, W.: Urban growth and aerosol effects on convection over Houston. Part II: Dependence of aerosol effects on instability, Atmospheric research, 102, 167–174, 2011.

Ceppi, P., Brient, F., Zelinka, M. D., and Hartmann, D. L.: Cloud feedback mechanisms and their representation in global climate models, Wiley Interdisciplinary Reviews: Climate Change, 8, e465, 2017.

Chen, Q., Koren, I., Altaratz, O., Heiblum, R. H., Dagan, G., and Pinto, L.: How do changes in warm-phase microphysics affect deep convective clouds?, Atmospheric Chemistry and Physics, 17, 9585–9598, 2017.

Christensen, M. W., Chen, Y.-C., and Stephens, G. L.: Aerosol indirect effect dictated by liquid clouds, Journal of Geophysical Research: Atmospheres, 121, 14–636, 2016.

Christensen, M. W., Gettelman, A., Cermak, J., Dagan, G., Diamond, M., Douglas, A., Feingold, G., Glassmeier, F., Goren, T., Grosvenor, D. P., et al.: Opportunistic experiments to constrain aerosol effective radiative forcing, Atmospheric chemistry and physics, 22, 641–674, 2022.

Collins, W. D., Rasch, P. J., Boville, B. A., Hack, J. J., McCaa, J. R., Williamson, D. L., Briegleb, B. P., Bitz, C. M., Lin, S.-J., and Zhang, M.: The formulation and atmospheric simulation of the Community Atmosphere Model version 3 (CAM3), Journal of Climate, 19, 2144–2161, 2006.

Dagan, G.: Equilibrium climate sensitivity increases with aerosol concentration due to changes in precipitation efficiency, Atmospheric Chemistry and Physics, 22, 15 767–15 775, 2022.

Dagan, G. and Stier, P.: Constraint on precipitation response to climate change by combination of atmospheric energy and water budgets, npj Climate and Atmospheric Science, 3, 1–5, 2020a.

Dagan, G. and Stier, P.: Ensemble daily simulations for elucidating cloud–aerosol interactions under a large spread of realistic environmental conditions, Atmospheric Chemistry and Physics, 20, 6291–6303, 2020b.

Dagan, G., Koren, I., and Altaratz, O.: Aerosol effects on the timing of warm rain processes, Geophysical Research Letters, 42, 4590–4598, 2015.

Dagan, G., Koren, I., Altaratz, O., and Heiblum, R. H.: Time-dependent, non-monotonic response of warm convective cloud fields to changes in aerosol loading, Atmospheric Chemistry and Physics, 17, 7435–7444, 2017.

Dagan, G., Koren, I., and Altaratz, O.: Quantifying the effect of aerosol on vertical velocity and effective terminal velocity in warm convective clouds, Atmospheric Chemistry and Physics, 18, 6761–6769, 2018.

https://doi.org/10.5194/egusphere-2023-2096
Preprint. Discussion started: 4 October 2023

Dagan, G., Stier, P., Christensen, M., Cioni, G., Klocke, D., and Seifert, A.: Atmospheric energy budget response to idealized aerosol perturbation in tropical cloud systems, Atmospheric Chemistry and Physics, 20, 4523–4544, 2020.

Dagan, G., Stier, P., Spill, G., Herbert, R., Heikenfeld, M., van den Heever, S. C., and Marinescu, P. J.: Boundary conditions representation can determine simulated aerosol effects on convective cloud fields, Communications Earth & Environment, 3, 1–7, 2022.

Fan, J., Comstock, J. M., and Ovchinnikov, M.: The cloud condensation nuclei and ice nuclei effects on tropical anvil characteristics and water vapor of the tropical tropopause layer, Environmental Research Letters, 5, 044 005, 2010.

Fan, J., Leung, L. R., Rosenfeld, D., Chen, Q., Li, Z., Zhang, J., and Yan, H.: Microphysical effects determine macrophysical response for aerosol impacts on deep convective clouds, Proceedings of the National Academy of Sciences, 110, E4581–E4590, 2013.

Freud, E. and Rosenfeld, D.: Linear relation between convective cloud drop number concentration and depth for rain initiation, Journal of Geophysical Research: Atmospheres, 117, 2012.

Gettelman, A. and Sherwood, S. C.: Processes responsible for cloud feedback, Current climate change reports, 2, 179–189, 2016.

Grabowski, W. W. and Morrison, H.: Untangling microphysical impacts on deep convection applying a novel modeling methodology. Part II: Double-moment microphysics, Journal of the Atmospheric Sciences, 73, 3749–3770, 2016.

Gryspeerdt, E. and Stier, P.: Regime-based analysis of aerosol-cloud interactions, Geophysical research letters, 39, 2012.

Hartmann, D. L. and Berry, S. E.: The balanced radiative effect of tropical anvil clouds, Journal of Geophysical Research: Atmospheres, 122, 5003–5020, 2017.

Hartmann, D. L. and Larson, K.: An important constraint on tropical cloud-climate feedback, Geophysical research letters, 29, 12–1, 2002.

Heikenfeld, M., White, B., Labbouz, L., and Stier, P.: Aerosol effects on deep convection: the propagation of aerosol perturbations through convective cloud microphysics, Atmospheric Chemistry and Physics, 19, 2601–2627, 2019.

Igel, A. L. and van den Heever, S. C.: Invigoration or Enervation of Convective Clouds by Aerosols?, Geophysical Research Letters, 48, e2021GL093 804, 2021.

Khairoutdinov, M. F. and Randall, D. A.: Cloud resolving modeling of the ARM summer 1997 IOP: Model formulation, results, uncertainties, and sensitivities, Journal of the Atmospheric Sciences, 60, 607–625, 2003.

Koren, I., Kaufman, Y. J., Rosenfeld, D., Remer, L. A., and Rudich, Y.: Aerosol invigoration and restructuring of Atlantic convective clouds, Geophysical Research Letters, 32, 2005.

Koren, I., Dagan, G., and Altaratz, O.: From aerosol-limited to invigoration of warm convective clouds, science, 344, 1143–1146, 2014.

Koren, I., Altaratz, O., and Dagan, G.: Aerosol effect on the mobility of cloud droplets, Environmental Research Letters, 10, 104 011, 2015.

Li, R., Storelvmo, T., Fedorov, A. V., and Choi, Y.-S.: A positive IRIS feedback: Insights from climate simulations with temperature-sensitive cloud–rain conversion, Journal of climate, 32, 5305–5324, 2019.

Lindzen, R. S., Chou, M.-D., and Hou, A. Y.: Does the earth have an adaptive infrared iris?, Bulletin of the American Meteorological Society, 82, 417–432, 2001.

Lutsko, N. J. and Cronin, T. W.: Increase in precipitation efficiency with surface warming in radiative-convective equilibrium, Journal of Advances in Modeling Earth Systems, 10, 2992–3010, 2018.

Mauritsen, T. and Stevens, B.: Missing iris effect as a possible cause of muted hydrological change and high climate sensitivity in models, Nature Geoscience, 8, 346–351, 2015.

Morrison, H., Curry, J., and Khvorostyanov, V.: A new double-moment microphysics parameterization for application in cloud and climate models. Part I: Description, Journal of the atmospheric sciences, 62, 1665–1677, 2005.

https://doi.org/10.5194/egusphere-2023-2096
Preprint. Discussion started: 4 October 2023

Muller, C. J. and Held, I. M.: Detailed investigation of the self-aggregation of convection in cloud-resolving simulations, Journal of the Atmospheric Sciences, 69, 2551–2565, 2012.

Muller, C. J. and O'Gorman, P.: An energetic perspective on the regional response of precipitation to climate change, Nature Climate Change, 1, 266–271, 2011.

Nuijens, L. and Siebesma, A. P.: Boundary layer clouds and convection over subtropical oceans in our current and in a warmer climate, Current Climate Change Reports, 5, 80–94, 2019.

Romps, D. M., Latimer, K., Zhu, Q., Jurkat-Witschas, T., Mahnke, C., Prabhakaran, T., Weigel, R., and Wendisch, M.: Air pollution unable to intensify storms via warm-phase invigoration, Geophysical Research Letters, p. e2022GL100409, 2023.

Rosenfeld, D.: Suppression of rain and snow by urban and industrial air pollution, science, 287, 1793–1796, 2000.

Rosenfeld, D., Lohmann, U., Raga, G. B., O'Dowd, C. D., Kulmala, M., Fuzzi, S., Reissell, A., and Andreae, M. O.: Flood or drought: how do aerosols affect precipitation?, science, 321, 1309–1313, 2008.

Saint-Lu, M., Bony, S., and Dufresne, J.-L.: Observational evidence for a stability iris effect in the tropics, Geophysical Research Letters, 47, e2020GL089 059, 2020.

Seeley, J. T., Jeevanjee, N., Langhans, W., and Romps, D. M.: Formation of tropical anvil clouds by slow evaporation, Geophysical Research Letters, 46, 492–501, 2019.

Seifert, A. and Beheng, K.: A two-moment cloud microphysics parameterization for mixed-phase clouds. Part 2: Maritime vs. continental deep convective storms, Meteorology and Atmospheric Physics, 92, 67–82, 2006.

Seinfeld, J. H., Bretherton, C., Carslaw, K. S., Coe, H., DeMott, P. J., Dunlea, E. J., Feingold, G., Ghan, S., Guenther, A. B., Kahn, R., et al.: Improving our fundamental understanding of the role of aerosol- cloud interactions in the climate system, Proceedings of the National Academy of Sciences, 113, 5781–5790, 2016.

Sokol, A. B. and Hartmann, D. L.: "No evidence for negative anvil cloud feedback in high-resolution models" by, 2023.

Squires, P.: The microstructure and colloidal stability of warm clouds: Part I—The relation between structure and stability, Tellus, 10, 256–261, 1958.

Squires, P. and Twomey, S.: The relation between cloud droplet spectra and the spectrum of cloud nuclei, Geophysical Monograph Series, 5, 211–219, 1960.

Stevens, B. and Feingold, G.: Untangling aerosol effects on clouds and precipitation in a buffered system, Nature, 461, 607–613, 2009.

Twomey, S.: The nuclei of natural cloud formation part II: The supersaturation in natural clouds and the variation of cloud droplet concentration, Geofisica pura e applicata, 43, 243–249, 1959.

Twomey, S.: Pollution and the planetary albedo, Atmospheric Environment (1967), 8, 1251–1256, 1974.

Twomey, S.: The influence of pollution on the shortwave albedo of clouds, Journal of the atmospheric sciences, 34, 1149–1152, 1977.

Varble, A.: Erroneous attribution of deep convective invigoration to aerosol concentration, Journal of the Atmospheric Sciences, 75, 1351–1368, 2018.

Williams, A. I., Watson-Parris, D., Stier, P., and Dagan, G.: Dependence of fast changes in global and local precipitation on the geographical location of aerosol absorption, Authorea Preprints, 2023.

Williams, E., Rosenfeld, D., Madden, N., Gerlach, J., Gears, N., Atkinson, L., Dunnemann, N., Frostrom, G., Antonio, M., Biazon, B., et al.: Contrasting convective regimes over the Amazon: Implications for cloud electrification, Journal of Geophysical Research: Atmospheres, 107, LBA–50, 2002.

https://doi.org/10.5194/egusphere-2023-2096
Preprint. Discussion started: 4 October 2023

Williams, I. N. and Pierrehumbert, R. T.: Observational evidence against strongly stabilizing tropical cloud feedbacks, Geophysical Research Letters, 44, 1503–1510, 2017.

Wing, A. A., Reed, K. A., Satoh, M., Stevens, B., Bony, S., and Ohno, T.: Radiative–convective equilibrium model intercomparison project, Geoscientific Model Development, 11, 793–813, 2018.

Wing, A. A., Stauffer, C. L., Becker, T., Reed, K. A., Ahn, M.-S., Arnold, N. P., Bony, S., Branson, M., Bryan, G. H., Chaboureau, J.-P., et al.: Clouds and convective self-aggregation in a multimodel ensemble of radiative-convective equilibrium simulations, Journal of advances in modeling earth systems, 12, e2020MS002 138, 2020.

Yuan, T., Remer, L. A., Pickering, K. E., and Yu, H.: Observational evidence of aerosol enhancement of lightning activity and convective invigoration, Geophysical Research Letters, 38, 2011.

Zelinka, M. D. and Hartmann, D. L.: Why is longwave cloud feedback positive?, Journal of Geophysical Research: Atmospheres, 115, 2010.

Zelinka, M. D. and Hartmann, D. L.: The observed sensitivity of high clouds to mean surface temperature anomalies in the tropics, Journal of Geophysical Research: Atmospheres, 116, 2011.